Acta Mech 227, 1393–1413 (2016)
DOI 10.1007/s00707-016-1560-2

ORIGINAL PAPER

Anil Misra · Payam Poorsolhjouy

Granular micromechanics model of anisotropic elasticity derived from Gibbs potential

Received: 26 August 2015 / Revised: 18 December 2015 / Published online: 1 February 2016

Abstract This paper presents a Gibbs potential-based granular micromechanics approach capable of modeling materials with complete anisotropy. The deformation energy of each grain–pair interaction is taken as a function of the inter-granular forces. The overall classical Gibbs potential of a material point is then defined as the volume average of the grain–pair deformation energy. As a first-order theory, the inter-granular forces are related to the Cauchy stress tensor using a modified static constraint that incorporates directional distribution of the grain–pair interactions. Further considering the conjugate relationship of the macroscale strain tensor and the Cauchy stress, a relationship between inter-granular displacement and the strain tensor is derived. To establish the constitutive relation, the inter-granular stiffness coefficients are introduced considering the conjugate relation of inter-granular displacement and forces. Notably, the inter-granular stiffness introduced in this manner is by definition different from that of the isolated grain–pair interactive. The integral form of the constitutive relation is then obtained by defining two directional density distribution functions; one related to the average grain–scale combined mechanical–geometrical properties and the other related to purely geometrical properties. Finally, as the main contribution of this paper, the distribution density function is parameterized using spherical harmonics expansion with carefully selected terms that has the capability of modeling completely anisotropic (triclinic) materials. By systematic modification of this distribution function, different elastic symmetries ranging from isotropic to completely anisotropic (triclinic) materials are modeled. As a comparison, we discuss the results of the present method with those obtained using a kinematic assumption for the case of isotropy and transverse isotropy, wherein it is found that the velocity of surface quasi-shear waves can show different trends for the two methods.

1 Introduction

Many materials show direction-dependent response to loading or anisotropic behavior at their so-called macroscale. In the broadest scheme, the directional dependency of material behavior is categorized into two major categories, namely *inherent* anisotropy and *induced* anisotropy. If the material shows direction-dependent response to loading from the initial unloaded state, it is said to have inherent anisotropy. These include granular materials in which inter-granular mechanisms in different directions are not the same, multiphase the material and materials with microcracks and fissures [1–6]. A direction-dependent nature of the

A. Misra (✉) · P. Poorsolhjouy
Civil, Environmental and Architectural Engineering Department, University of Kansas, 1530 W. 15th Street, Learned Hall, Lawrence, KS 66045-7609, USA
E-mail: amisra@ku.edu
Tel.: (785) 864-1750
Fax: (785) 864-5631

A. Misra
Department of Civil Engineering, Shanghai Jiao Tong Univ., Dong Chuan Rd., Shanghai 200240, China

material response to loading is enhanced further by the effect of loading, even for initially (*inherently*) isotropic materials. As loading progresses and the material is no longer in its initial unloaded state, different microscale mechanisms in different directions lead to the evolution of directional-dependent material behavior. These phenomena include, but are not limited to, change of the inter-particle interactions, change in the shapes and sizes of particles, change in the distribution of crystalline directions in polycrystalline materials, change of surface properties, change of contacts, damage and fracture, pore collapse, bond breakage, hardening or softening of the generally nonlinear inter-particle behavior. Accumulation of effects of these phenomena results in enhanced direction-dependent behavior, which is usually referred to as *induced* anisotropy [7–14].

A robust material model should be able to capture the anisotropy of material behavior. One of the most promising approaches for predicting the behavior of this class of materials is using micromechanical models where microscale and macroscale are related to each other using a proper set of assumptions with constitutive laws defined in microscopic scale. This allows for the constitutive laws to represent more conveniently the directional properties of the material. The granular micromechanics approach, first introduced by Chang and Misra [15] and traceable to works of Navier [16] and Cauchy [17], is a very effective method for imposing micromechanical properties of the material onto the macroscopic behavior of the material. In this approach, the material RVE is assumed to be composed of a set of grains interacting with each other through different inter-granular mechanisms characterizing the material's macroscopic behavior [18]. Constitutive laws in microscopic scale are written relating local inter-granular displacement and force components, and the macroscopic behavior of the material is derived by calculating the macroscopic free energy density as the volume average of grain–pair interaction energies. The approach is consistent with the idea of coarse graining for modeling polymeric or complex multiatomic systems [19–21] and follows a similar paradigm as that of peridynamics [22,23] and quasi-continuum mechanics [24]. The method also bears similarity to the microplane model [25] and the virtual internal bond (VIB) model [26] where the material behavior is derived considering the behavior of planes or bonds of every generic orientation.

Micromechanical models of this type in general need an assumption by which the macroscopic stress or strain tensors are transformed into microscopic force or displacement vectors [27–30]. Methods are typically divided into two categories, namely methods with a kinematic assumption and methods with a static assumption. The kinematic assumption maintains that the inter-granular displacements in any direction are derived as projections of the strain tensor in that particular direction. On the other hand, the static assumption, traditionally, assumes the inter-particle force vector to be the projection of stress tensor in the direction of the contact. Over the years, these assumptions have been refined by considering more carefully the transmission of local contact forces [31,32] or by introduction of mesoscale consisting of particle clusters [32–36]. Here, we utilize a modified static assumption, wherein the inter-granular force vector is found through minimizing an error function in a least squares approximation scheme for inter-granular displacements [37]. The present work further develops the framework of granular micromechanics based upon the classical Gibbs potential to address the following three aspects: (1) interpretation of inter-granular interaction by considering the conjugate relationships of inter-granular displacements and forces, which shows that the inter-granular stiffness/compliance coefficients introduced in continuum models are by definition different from that of isolated grain–pair, (2) derivation of an integral form for the compliance tensor by introducing two distinct directional density distribution functions; one related to the average grain–scale combined mechanical–geometrical properties and the other related to purely geometrical properties, and finally, (3) the key focus on parameterization of distribution density function using spherical harmonics expansion for modeling all different levels of anisotropy ranging from isotropic to triclinic.

Modeling of anisotropic materials within micromechanical methods has been attempted in the past, particularly based upon the microplane model. In these efforts, anisotropy is typically modeled by defining microscopic stiffness coefficients as functions of the microplane or contact direction [38,39]. More recently, the spectral decomposition approach has been presented for representing material anisotropy [40]. The spectral decomposition approach has been successfully applied to model transversely isotropic and orthotropic materials. However, the method has not been applied to materials with higher level of anisotropy (namely materials with only one plane of elastic symmetry and completely anisotropic materials with no elastic symmetry). The present work describes a comprehensive approach that can systematically describe material symmetries ranging from isotropic to completely anisotropic (triclinic). To capture the mechanical properties of a completely anisotropic material, we introduce three distinct microscopic stiffness coefficients to model the deformation energy of interacting grain–pairs. Further, directional density distribution functions are defined, which take into account the directional distribution of number, length, and stiffness/compliance of grain–pair interactions. The density distribution functions enable the constitutive relationship to be expressed in an integral form. For

closed-form derivation of expressions for the anisotropic elastic constants, the directional density distribution function is parameterized using spherical harmonics expansion. By progressively including additional terms in the parameterized distribution function, the method is enabled to model materials with different levels of anisotropy. The effect of model's microscale parameters on the macroscopic behavior of anisotropic materials is demonstrated using two different measures. First, elastic wave velocity [41] is discussed and its variation by changing micromechanical parameters is shown. In addition, results of the present approach are compared to those of the method using kinematic constraint for transversely isotropic materials and also isotropic materials. Then, as a measure of the severity of the material's anisotropy, the universal anisotropy index [42] is discussed. These phenomena show the effectiveness of the present approach in modeling the behavior of inherently anisotropic materials.

2 Granular micromechanics method using Gibbs potential

The deformation energy of an RVE of a granular material can be written in terms of the deformation energies of the grain–pair interactions. For continuum modeling, the RVE deformation energy is typically formulated in terms of stresses and strains. The deformation energy of the grain–pair interactions, on the other hand, is more conveniently formulated in terms of forces and displacements. The key problem remains the identification of the stress–force and the strain–displacement measures (or micro–macro measures) at these two scales and may require the introduction of additional measures beyond the classical terms as has been discussed in recent works related to a micromorphic model of granular media [18,43]. The existence of higher-order or hyperstress and its significance has been recognized [44,45], particularly for the case of granular materials under elastic deformation (see for example [18,46,47] among others) In recent years, the formulation of hyperstress from the arguments of Cauchy format of continuum theory has also been shown to be valid and reconciled with the formulation that follows from D'Alembert postulations [48–51]. Here we consider only the first-order terms for illustration of approach to focus the discussion upon the three goals stated in the Introduction. Thus, we consider the classical Gibbs potential, G, of an RVE of a granular material defined in terms of the Cauchy stress and its conjugate strain. The RVE Gibbs potential can be obtained as the volume density of the grain–pair interactions as follows:

$$G = \frac{1}{V}\sum_{\alpha}^{N} G^{\alpha}\left(f_j^{\alpha}\right), \tag{1}$$

where N is the total number of grain–pair interactions in the RVE and $G^{\alpha}\left(f_j^{\alpha}\right)$ is the deformation energy of the αth grain–pair interaction given in terms of the grain–pair force, f_j^{α}, and the conjugate inter-granular elastic displacement, δ_j^{α}, as

$$\delta_j^{\alpha} = \frac{\partial G^{\alpha}}{\partial f_j^{\alpha}}. \tag{2}$$

To establish the grain–pair conjugate force and deformation measures in terms of the macroscale quantities, the conjugate relationship of the macroscale strain, ε_{ij}, and Cauchy stress tensor, σ_{ij}, can be combined with Eq. (1) and the chain rule of differentiation to find

$$\varepsilon_{ij} = \frac{\partial G}{\partial \sigma_{ij}} = \frac{1}{V}\sum_{\alpha=1}^{N} \frac{\partial G^{\alpha}}{\partial f_k^{\alpha}}\frac{\partial f_k^{\alpha}}{\partial \sigma_{ij}}. \tag{3}$$

We note here that the assumed classical Gibbs potential formulation has important consequences that have not been recognized in previous works that report similar final formulation of the constitutive relations [28, 52,53], but become significant when inter-granular stiffness coefficients are defined considering the conjugate relationship of inter-granular displacement and forces. The inter-granular stiffness coefficients introduced in this manner are by definition different from that of isolated grain–pair and may not be obtained by considering the mechanics of grains isolated from their material environment.

Further, the inter-granular force vector in many traditional statically constrained methods is taken as the projection of the stress tensor in the direction of grain–pair interaction. Here, we utilize the results from a least squares approximation for inter-granular displacements to enhance this assumption considering the directional distribution of the grain–pair interactions [28,37,54], which gives the following relationship between the

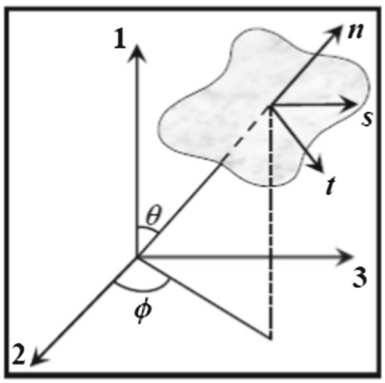

Fig. 1 Local inter-granular Cartesian coordinates shown at an intergranular contact location

grain–pair force, f_j^α, and the Cauchy stress tensor (see the Appendix: least squares approximation for a brief derivation):

$$f_i^\alpha = l^\alpha \sigma_{ij} N_{jr}^{-1} n_r^\alpha, \tag{4}$$

where l^α is the length of the branch vector joining the centroids of two neighbor grains $l_r^\alpha = l^\alpha n_r^\alpha$, and N_{ij} is a fabric tensor given by

$$N_{ij} = \frac{1}{V} \sum_{\alpha=1}^{N} l_i^\alpha l_j^\alpha. \tag{5}$$

Substituting Eq. (2) and (4) into Eq. (3), the relationship between the inter-granular displacement, δ_j^α, and the strain tensor is obtained as

$$\varepsilon_{ij} = \frac{\partial G}{\partial \sigma_{ij}} = \frac{1}{V} \sum_{\alpha=1}^{N} \delta_i^\alpha l^\alpha N_{jk}^{-1} n_k^\alpha = \frac{N_{jk}^{-1}}{V} \sum_{\alpha=1}^{N} \delta_i^\alpha l^\alpha n_k^\alpha. \tag{6}$$

A microscale constitutive equation is now introduced at the grain–scale to relate the inter-granular force and displacement measures. To simplify the inter-granular force–displacement relationships, a local coordinate system is defined for each interacting grain–pair. The coordinate system, as it is seen in Fig. 1, is composed of three mutually orthogonal unit vectors. These include one normal vector, $\boldsymbol{n}$, in the direction of the branch vector joining the centroids of the two grains and two vectors orthogonal to the normal vector and lying in the tangential plane between the two interacting grains, $\boldsymbol{s}$ and $\boldsymbol{t}$,

$$\begin{aligned} n_i &= \langle \cos\theta, \sin\theta\cos\phi, \sin\theta\sin\phi \rangle, \\ s_i &= \langle -\sin\theta, \cos\theta\cos\phi, \cos\theta\sin\phi \rangle, \\ t_i &= \langle 0, -\sin\phi, \cos\phi \rangle, \end{aligned} \tag{7}$$

where θ and ϕ are the polar and azimuth angles in the spherical coordinate system, respectively.

Using this local coordinate system, the inter-granular displacement vector is decomposed into components in the normal and tangential directions:

$$\delta_n^\alpha = \delta_i^\alpha n_i^\alpha; \quad \delta_s^\alpha = \delta_i^\alpha s_i^\alpha; \quad \delta_t^\alpha = \delta_i^\alpha t_i^\alpha. \tag{8}$$

Thus, the constitutive equation at the grain–scale can be written as follows:

$$\left\{\delta^\alpha\right\}_{3\times1} = \left[s^\alpha\right]_{3\times3} \left\{f^\alpha\right\}_{3\times1}; \quad \begin{Bmatrix} \delta_n^\alpha \\ \delta_s^\alpha \\ \delta_t^\alpha \end{Bmatrix} = \begin{bmatrix} 1/k_n^\alpha & 0 & 0 \\ 0 & 1/k_s^\alpha & 0 \\ 0 & 0 & 1/k_t^\alpha \end{bmatrix} \begin{Bmatrix} f_n^\alpha \\ f_s^\alpha \\ f_t^\alpha \end{Bmatrix}, \tag{9}$$

where k_n, k_s and k_t are the stiffness coefficients and the matrix $[s]$ is the compliance matrix. We note here that these stiffness coefficients do not represent the stiffness of isolated grain-pairs. Instead, they model the behavior of a grain-pair embedded in a granular material and represent the effect of immediate neighbors as well as the

entire microstructure as revealed in the equilibrium analysis of grain assemblies subjected to uniform boundary displacements [34]. The general nature of inter-granular stiffness is also clear from kinematic analysis valid for micromorphic models of granular media [18]. These stiffness coefficients function as parameters that need to be determined as back-calculations from macroscale measurements. It is also notable that in Eq. (9) the inter-granular constitutive relation is defined in a linear fashion, and the coupling between normal and tangential components of force and displacement vectors is not taken into account. For nonlinear materials, the inter-granular constitutive relation may be generalized to be nonlinear, including coupling terms in the microscale [37,55–57].

The microscale constitutive law can be transformed into the RVE coordinate system using the following rotation tensor:

$$T = \begin{pmatrix} n_1 & s_1 & t_1 \\ n_2 & s_2 & t_2 \\ n_3 & s_3 & t_3 \end{pmatrix}, \tag{10}$$

where the components of the rotation tensor are the components of the unit vectors in the local coordinate system. The microscale constitutive relation in the RVE coordinate system will be rewritten as

$$\delta_i^\alpha = S_{ij}^\alpha f_j^\alpha; \quad S_{ij}^\alpha = T_{ip}^\alpha s_{pq}^\alpha T_{jq}^\alpha. \tag{11}$$

The second rank tensor s_{pq}^α in the second part of Eq. (11) is the compliance tensor of the αth grain–pair interaction in the contacts' local coordinate system (the coordinate system defined by the unit normal vector, $\boldsymbol{n}$, and the two tangential unit vectors, $\boldsymbol{s}$ and $\boldsymbol{t}$) while the tensor S_{ij}^α is the compliance tensor in the RVE coordinate system (with the unit vectors $\boldsymbol{1}$, $\boldsymbol{2}$, and $\boldsymbol{3}$). Now substituting Eq. (4) along with Eq. (11) into the expression derived for macroscopic strain, Eq. (6), and noting that the macroscopic stress tensor does not depend upon grain–pair, the relationship between macroscopic strain tensor and the Cauchy stress is found to be

$$\varepsilon_{ij} = \left(\frac{N_{jr}^{-1} N_{lq}^{-1}}{V} \sum_{\alpha=1}^{N} l^2 S_{ik}^\alpha n_r^\alpha n_q^\alpha \right) \sigma_{kl}, \tag{12}$$

and consequently, the compliance tensor is written as

$$S_{ijkl} = \frac{N_{jr}^{-1} N_{ls}^{-1}}{V} \sum_{\alpha=1}^{N} l^2 S_{ik}^\alpha n_r^\alpha n_s^\alpha. \tag{13}$$

Using Eq. (11), Eq. (13) can be expressed as

$$S_{ijkl} = \frac{N_{jr}^{-1} N_{lq}^{-1}}{V} \sum_{\alpha=1}^{N} n_r^\alpha n_q^\alpha \left(\left(l^\alpha\right)^2 \frac{1}{k_n^\alpha} n_i^\alpha n_k^\alpha + \left(l^\alpha\right)^2 \frac{1}{k_s^\alpha} s_i^\alpha s_k^\alpha + \left(l^\alpha\right)^2 \frac{1}{k_t^\alpha} t_i^\alpha t_k^\alpha \right), \tag{14}$$

where summations are over all grain–pair interactions in the RVE. Note that throughout this paper, the subscripts n, s, and t represent the inter-granular properties, which are normal ($\boldsymbol{n}$), and tangential ($\boldsymbol{s}$ and $\boldsymbol{t}$) directions, respectively, and thus do not follow the index notation conventions.

For an RVE containing many ($>10^6$) interacting grains, the exact knowledge of the material composition and properties, grain shapes and sizes, interfacial properties, etc. is unknown. Such detailed information is generally unattainable for almost all engineering materials. Therefore, the precise and true nature of every grain–pair interaction is unknown. However, this unfortunately missing information is compensated by the fortunate fact that generally for the determination of collective behavior we are not interested in the precise and detailed solution for the exact motion of each and every grain in the RVE. In this work, we have chosen to treat the problem in a statistical sense by considering mean behaviors. Such statistical approximations are reasonably justified when firstly there is the absence of complete information about the microstructure and the micromechanical parameters, and secondly, an incomplete solution, such as the mean behavior, based upon incomplete data is sufficient. With the aim of obtaining the estimate of the mean behavior, Eq. (14) can be rewritten, observing that the terms in the summation are products of the direction cosines, the branch length and compliances associated with grain–pairs, which can be binned into discrete solid angles. Thus, the summation in Eq. (14), over the total number of contacts within the system, can be rewritten as a summation over θ and ϕ as

$$S_{ijkl} = \frac{N_{jr}^{-1} N_{lq}^{-1}}{V} \sum_{\theta} \sum_{\phi} \left[\left(\sum_{\rho} \frac{(l^{\rho})^2}{k_n^{\rho}} \right) n_r n_q n_i n_k + \left(\sum_{\rho} \frac{(l^{\rho})^2}{k_s^{\rho}} \right) n_r n_q s_i s_k + \left(\sum_{\rho} \frac{(l^{\rho})^2}{k_t^{\rho}} \right) n_r n_q t_i t_k \right], \tag{15}$$

where the three summations over ρ represent summations over all inter-granular contacts whose orientation lies in a given solid angle range centered at θ and ϕ. For example, the term $\sum_{\rho} (l^{\rho})^2 / k_n^{\rho}$ represents the sum of $(l^{\rho})^2 / k_n^{\rho}$ terms for all grain–pair interactions whose orientations are contained within a given solid angle range. For anisotropic materials, these sums will be different for different solid angles, which can be expediently treated by defining directional distribution functions. Since branch length and compliances appear as products, their directional distribution density cannot be defined independently and the relevant quantity to use is the product of l^2 and the compliance coefficients ($1/k_n$, or $1/k_s$, or $1/k_t$). To this end, we introduce directional density distribution function, $\xi(\theta, \phi)$, which represents the directional distribution of the number, length, and stiffness of grain–pair interactions as follows:

$$\frac{\sum_{\rho} (l^{\rho})^2 / k_n^{\rho}}{\sum_{\alpha=1}^{N} (l^{\alpha})^2 / k_n^{\alpha}} = \frac{\sum_{\rho} (l^{\rho})^2 / k_s^{\rho}}{\sum_{\alpha=1}^{N} (l^{\alpha})^2 / k_s^{\alpha}} = \frac{\sum_{\rho} (l^{\rho})^2 / k_t^{\rho}}{\sum_{\alpha=1}^{N} (l^{\alpha})^2 / k_t^{\alpha}} = \xi(\theta, \phi), \tag{16}$$

where it has been assumed that all the inter-granular compliances also follow the same distribution. In addition, it is useful to define an average value of the terms $\frac{(l^{\alpha})^2}{k_n^{\alpha}}$ (and similarly for the shear terms) as

$$\frac{\sum_{\alpha=1}^{N} (l^{\alpha})^2 / k_n^{\alpha}}{N} = l^2 / k_n; \quad \frac{\sum_{\alpha=1}^{N} (l^{\alpha})^2 / k_s^{\alpha}}{N} = l^2 / k_s; \quad \frac{\sum_{\alpha=1}^{N} (l^{\alpha})^2 / k_t^{\alpha}}{N} = l^2 / k_t, \tag{17}$$

where l^2/k_n, l^2/k_s, and l^2/k_t are average values for the RVE. Combining Eqs. (16) and (17) with Eq. (15), and defining ρ^c as the volume density of total number of grain–pair contacts ($\rho^c = N/V$), the compliance tensor given in Eq. (15) can be written in integral form as

$$\begin{aligned} S_{ijkl} &= l^2 \rho^c N_{jr}^{-1} N_{lq}^{-1} \int_{\theta=0}^{\pi} \int_{\phi=0}^{2\pi} \left(\frac{1}{k_n} n_r n_q n_i n_k + \frac{1}{k_s} n_r n_q s_i s_k + \frac{1}{k_t} n_r n_q t_i t_k \right) \xi(\theta, \phi) \sin\theta \, \mathrm{d}\phi \mathrm{d}\theta \\ &= l^2 \rho^c N_{jr}^{-1} N_{lq}^{-1} \int_{\theta=0}^{\pi} \int_{\phi=0}^{2\pi} \left(S_{ik} n_r n_q \right) \xi(\theta, \phi) \sin\theta \, \mathrm{d}\phi \mathrm{d}\theta, \end{aligned} \tag{18}$$

where it is noteworthy that the fabric tensor, N_{ij}, introduced in Eq. (5) can also be treated from a statistical viewpoint such that the summation in Eq. (5), over the total number of contacts within the system, can be rewritten as a summation over θ and ϕ in a manner similar to Eq. (15):

$$N_{ij} = \frac{1}{V} \sum_{\alpha=1}^{N} l_i^{\alpha} l_i^{\alpha} = \frac{1}{V} \sum_{\theta} \sum_{\phi} \left(\sum_{\rho} \left(l^{\rho} \right)^2 \right) n_i n_j. \tag{19}$$

Now, the average branch length l and the directional density distribution of number and length of the grain–pair interactions, $\xi'(\theta, \phi)$, may be introduced:

$$\frac{\sum_{\alpha=1}^{N} (l^{\alpha})^2}{N} = l^2; \quad \frac{\sum_{\rho} (l^{\rho})^2}{\sum_{\alpha=1}^{N} (l^{\alpha})^2} = \xi'(\theta, \phi). \tag{20}$$

As a result, the second rank fabric tensor given in Eq. (19) can be written in an integral form as

$$N_{ij} = \rho^c \int_{\theta=0}^{2\pi} \int_{\phi=0}^{\pi} l_i l_j \xi'(\theta, \phi) \sin\theta \, \mathrm{d}\theta \mathrm{d}\phi = l^2 \rho^c \int_{\theta=0}^{2\pi} \int_{\phi=0}^{\pi} n_i n_j \xi'(\theta, \phi) \sin\theta \, \mathrm{d}\theta \mathrm{d}\phi. \tag{21}$$

It is noteworthy that the two directional density distribution functions, $\xi(\theta, \phi)$ and $\xi'(\theta, \phi)$, are distinct since they represent the distribution of different parameters, in contrast to the assumption widely made in previous

derivations of this type [28,52,54]. However, for simplicity of subsequent discussion and calculations, the two directional density distribution functions are assumed to be the same in the remainder of this paper where the focus is on elastic behavior. For inelastic behavior, the use of distinct distributions may be representative as observed from the analysis of regular grain assemblies using the described approach in [37], wherein the stiffness coefficients of grain–contacts in different directions evolves with loading while the microstructure or fabric persists.

The fourth rank compliance tensor, S_{ijkl}, in its most general form has $3^4 = 81$ independent constants. However, symmetry of stress and strain tensors leads to minor symmetries of compliance tensor, and the constitutive equations can then be written in Voigt notation [58]. In this manner, the compliance tensor can be written as a 6×6 matrix with 36 components. The components of such compliance matrix are calculated as follows:

$$\gamma_{ij} = \varepsilon_{ij} + \varepsilon_{ji} = \left[\left(S_{ijkl} + S_{ijlk}\right) + \left(S_{jikl} + S_{jilk}\right)\right] \frac{\sigma_{kl} + \sigma_{lk}}{2} + \left[\left(S_{ijkl} + S_{ijlk}\right) - \left(S_{jikl} + S_{jilk}\right)\right] \frac{\sigma_{kl} - \sigma_{lk}}{2}. \tag{22}$$

In this equation, shear strain is taken as $\gamma_{ij} = \varepsilon_{ij} + \varepsilon_{ji}$. Further, average value of the two shear stresses is taken as the Cauchy stress, and the difference, $\sigma_{kl} - \sigma_{lk}$, is discarded. After constructing the 6×6 compliance matrix with this approach, major symmetry ($S_{ijkl} = S_{klij}$) is also applied on the compliance matrix, implying that the 6×6 matrix is also symmetric and has only 21 independent constants. The macroscopic stiffness matrix can also be derived as the inverse of the global compliance tensor. It should be noted that since the grain–scale constitutive equations, given in Eqs. (9) and (11), are linear, the macroscopic compliance and stiffness tensors are also linear. More complicated inter-granular constitutive relationships have been used for modeling nonlinear behavior of a wide range of materials and for different loading conditions [37,55–57].

3 Directional dependence using density distribution function

The anisotropy arising from a smooth variation of grain–pair properties can be represented using a directional density distribution function expressed as spherical harmonic first introduced in these types of model by Chang and Misra [15], given as

$$\xi(\theta, \phi) = \frac{1}{4\pi} \left\{ 1 + {\sum_{k=2}^{\infty}}' \left[a_{k0} P_k(\cos\theta) + \sum_{m=1}^{\infty} P_k^m(\cos\theta) \left(a_{km} \cos m\phi + b_{km} \sin m\phi\right) \right] \right\}, \tag{23}$$

where $P_k(\cos\theta)$ is the kth Legendre polynomial with respect to $\cos\theta$ and $P_k^m(\cos\theta)$ is its mth associated Legendre function. In this function, a_{k0}, a_{km}, and b_{km} are directional density parameters, which govern the directional dependence of the properties of grain–pair interactions. The summation over k (shown by Σ') is performed only with respect to even indices of k. All the terms in this function are orthogonal to one regardless of their coefficient. So the integral of the directional density distribution function given in Eq. (23) over a complete unit sphere is always equal to one regardless of the number of terms included in the function and the values of directional density parameters $\int_\theta \int_\phi \xi(\theta, \phi) \sin\theta \mathrm{d}\theta \mathrm{d}\phi = 1$.

It is shown here that by incorporating the first three harmonics expansions ($k = 2, 4, 6$) the method is able to capture all components of stiffness matrix of a completely anisotropic material. The directional density parameters needed for modeling complete anisotropy are a_{20}, a_{40}, a_{22}, a_{42}, a_{44}, a_{64}, b_{22}, b_{42}, b_{44}, b_{64}, b_{21}, b_{41}, b_{43}, b_{63}, a_{21}, a_{41}, a_{43}, and a_{63}. Using these eighteen fabric parameters along with the three microscopic inter-granular compliance coefficients (one in normal direction and two in tangential directions), the method will have a total of 21 parameters, which is consistent with the number of independent components of the stiffness/compliance matrix of completely anisotropic materials. Thus, the most general form of the density distribution function needed is given as

$$\xi_{(\theta,\phi)} = \frac{1}{4\pi} \left(1 + a_{20} \frac{3\cos^2\theta - 1}{2} + a_{40} \frac{35\cos^4\theta - 30\cos^2\theta + 3}{8} + a_{22}(3\sin^2\theta \cos 2\phi) + a_{42} \left(\frac{105\cos^2\theta - 15}{2} \sin^2\theta \cos 2\phi \right) + a_{44}(105\sin^4\theta \cos 4\phi) \right.$$

$$
\begin{aligned}
&+ a_{64}\left(\frac{83160\cos^2\theta - 7560}{16}\sin^4\theta\cos 4\phi\right) + b_{22}(3\sin^2\theta\sin 2\phi)\\
&+ b_{42}\left(\frac{105\cos^2\theta - 15}{2}\sin^2\theta\sin 2\phi\right) + b_{44}(105\sin^4\theta\sin 4\phi)\\
&+ b_{64}\left(\frac{83160\cos^2\theta - 7560}{16}\sin^4\theta\sin 4\phi\right) + a_{21}(-3\sin\theta\cos\theta\cos\phi)\\
&+ a_{41}\left(\frac{-35\cos^3\theta + 15\cos\theta}{2}\sin\theta\cos\phi\right) + a_{43}(-105\cos\theta\sin^3\theta\cos 3\phi)\\
&+ a_{63}\left(-\frac{27720\cos^3\theta - 7560\cos\theta}{16}\sin^3\theta\cos 3\phi\right) + b_{21}(-3\sin\theta\cos\theta\sin\phi)\\
&+ b_{41}\left(\frac{-35\cos^3\theta + 15\cos\theta}{2}\sin\theta\sin\phi\right) + b_{43}(-105\cos\theta\sin^3\theta\sin 3\phi)\\
&+ b_{63}\left(-\frac{27720\cos^3\theta - 7560\cos\theta}{16}\sin^3\theta\sin 3\phi\right)\Bigg). \qquad (24)
\end{aligned}
$$

The components of the fabric tensor for the fully anisotropic material, derived by substituting the directional density distribution function in Eq. (24) into Eq. (21), are as follows

$$
N_{ij} = \frac{l^2\rho^c}{15}\begin{pmatrix} 2a_{20}+5 & -3a_{21} & -3b_{21} \\ -3a_{21} & -a_{20}+6a_{22}+5 & 6b_{22} \\ -3b_{21} & 6b_{22} & -a_{20}-6a_{22}+5 \end{pmatrix}. \qquad (25)
$$

It is seen here that, although the complete $\xi(\theta,\phi)$ function given in Eq. (24) is used in calculating the fabric tensor, only the terms from the first harmonics expansion (terms with $k = 2$ in Eq. (25)) appear in after the integration. The derived fabric tensor is used in Eq. (18) for calculating the compliance tensor for the completely anisotropic material. For modeling materials with any level of isotropy, the distribution function needs to be modified based on their corresponding elastic symmetries.

4 Modeling materials with different levels of anisotropy

The model takes its simplest form for isotropic materials. In these materials, all planes are planes of elastic symmetry and all axes are axes of rotational symmetry. In macroscale, the material has the same properties in all directions. It is expected that in an isotropic material, the grain–pair interactions in different directions within the tangential plane should be identical. As a result, the two tangential inter-granular stiffness coefficients will be identical ($k_s = k_t$). Further, it should be noted that the grain–pair interactions in different directions should also be identical. Thus, the distribution of number, length, and stiffness of inter-granular contacts in different directions should be constant (thus $\xi = 1/4\pi$). In this case, two micromechanical parameters, namely the normal and tangential inter-granular stiffness coefficients, are used for modeling isotropic materials. This is consistent with the macroscopic behavior of isotropic materials, which needs no more than two mechanical properties (E and ν).

If the material has three orthogonal planes of elastic symmetry and an axis of rotational symmetry, it is said to be transversely isotropic. In this case, the plane whose normal vector is the axis of rotational symmetry will be a plane of isotropy and the material behavior in all directions inside this plane will be identical. For pursuing the derivations and without loss of generality, it is assumed that the axis of rotational symmetry is axis 1. In this case, the behavior of material inside the 23 plane is isotropic. The material properties should not be a function of the azimuth angle, ϕ. The directional density distribution function will thus be a function of only the polar angle, θ, and the only directional density parameters used for modeling transversely isotropic materials will be a_{k0}. The density distribution function used for these materials can be found from Eq. (24) and by setting all directional density parameters except for a_{20} and a_{40} equal to zero. In the inter-granular scale, the tangential plane should in general have different stiffness coefficients in different directions such that $k_s \neq k_t$. It is seen that the model uses three inter-granular stiffness coefficients and two directional density parameters for modeling these materials, which is consistent with the macroscale stiffness tensors of these materials being composed of five independent constants.

If the material has two orthogonal planes of elastic symmetry, the third plane that is orthogonal to both of those two planes will also be a plane of elastic symmetry [59]. Materials with three orthogonal planes of elastic symmetry are termed as orthotropic. In their macroscopic stiffness matrix, these materials have nine independent stiffness components. For modeling this class of materials, the method needs to incorporate nine microscopic parameters in order to be able to reproduce nine independent macroscopic stiffness components. It is proved here that by including a_{22}, a_{42}, a_{44}, and a_{64} in addition to the previously introduced five microscopic parameters (used for transversely isotropic materials), the method can reproduce all the nine independent components of the macroscopic stiffness matrix of the material while maintaining all symmetry requirements.

For materials having only one plane of elastic symmetry, termed as monoclinic, the choice of geometric parameters to include in the model depends on the plane of elastic symmetry. In macroscale, the nonzero components of stiffness matrix of monoclinic materials depend on the Cartesian plane of elastic symmetry. If the material has elastic symmetry with respect to 23 plane, 13 plane, or 12 plane, its elastic stiffness matrix will be given by Eq. (26a), (26b), and (26c), respectively [59,60]:

$$C = \begin{bmatrix} c_{11} & c_{12} & c_{13} & c_{14} & 0 & 0 \\ & c_{22} & c_{23} & c_{24} & 0 & 0 \\ & & c_{33} & c_{34} & 0 & 0 \\ & & & c_{44} & 0 & 0 \\ & \text{symm.} & & & c_{55} & c_{56} \\ & & & & & c_{66} \end{bmatrix}; \tag{26a}$$

$$C = \begin{bmatrix} c_{11} & c_{12} & c_{13} & 0 & c_{15} & 0 \\ & c_{22} & c_{23} & 0 & c_{25} & 0 \\ & & c_{33} & 0 & c_{26} & 0 \\ & & & c_{44} & 0 & c_{46} \\ & \text{symm.} & & & c_{55} & 0 \\ & & & & & c_{66} \end{bmatrix}; \tag{26b}$$

$$C = \begin{bmatrix} c_{11} & c_{12} & c_{13} & 0 & 0 & c_{16} \\ & c_{22} & c_{23} & 0 & 0 & c_{26} \\ & & c_{33} & 0 & 0 & c_{36} \\ & & & c_{44} & c_{45} & 0 \\ & \text{symm.} & & & c_{55} & 0 \\ & & & & & c_{66} \end{bmatrix}. \tag{26c}$$

It should be noted that, in case the elastic symmetry plane is not one of the coordinate planes, the number of nonzero components in the stiffness matrix will increase; however, there will still be only 13 independent parameters in the stiffness matrix. For modeling this type of materials, the method needs to incorporate four additional directional density parameters other than the nine parameters used for orthotropic materials. For materials in which the 23 plane is the plane of elastic symmetry, b_{22}, b_{42}, b_{44}, and b_{64} are added to the previous 9 microscopic constants. If the plane of elastic symmetry is the 13 plane, b_{21}, b_{41}, b_{43}, and b_{63} and if it is the 12 plane, a_{21}, a_{41}, a_{43}, and a_{63} are added to the previous nine microscopic constants.

Completely anisotropic or triclinic materials have no plane of elastic symmetry and no axis of rotational symmetry. For these materials, it is necessary to include all the previously mentioned eighteen directional density parameters in the model. These along with the three inter-granular stiffness coefficients compose the 21 microscopic parameters needed to model the 21 independent components in their stiffness matrix.

5 Transverse isotropy and isotropy: closed-form coefficients

The macroscopic stiffness matrix for materials with different levels of anisotropy can be derived in closed form by inverting the compliance matrix derived in Eq. (18). Since the closed-form solutions for triclinic materials have large number of terms to be presented efficiently, for illustration purposes we present here only the stiffness coefficients for transversely isotropic and materials. It is seen that by including the first two harmonics with coefficients a_{20} and a_{40} the method can produce all the five independent components of the stiffness matrix of a transversely isotropic material while satisfying the symmetry requirements. The macroscopic stiffness matrix is found in the following form:

Table 1 List of parameters defined for showing components of stiffness matrix of anisotropic materials

A	$2k_n\,(2a_{20}+5)^2\,[21\,(k_n+4k_s)+k_n\,(3a_{20}-4a_{40})+k_s\,(4a_{40}-24a_{20})]$
B	$35\,(3k_n+2k_s)+k_n\,(15a_{20}-20a_{40})+k_s\,(20a_{20}+20a_{40}-14a_{20}^2)$
C	$k_n\,(a_{20}-5)^2\,\big[k_n^2\,(882\,(k_t+5k_s)+k_s\,(-252a_{20}-840a_{40}+168a_{20}a_{40}-126a_{20}^2)$
	$+k_t\,(252a_{20}-336a_{40}-48a_{20}a_{40}+168a_{20}^2+32a_{40}^2))$
	$+k_nk_s\,(k_s\,(6615+2457a_{20}+840a_{40}-168a_{20}a_{40}-756a_{20}^2)$
	$+k_t\,(18081+2321a_{20}-3108a_{40}+96a_{20}a_{40}-36a_{20}^2-64a_{40}^2))$
	$+k_s^2k_t\,(14112+4032a_{20}+3444a_{40}-48a_{20}a_{40}-2628a_{20}^2+32a_{40}^2)\big]$
D	$k_n^2\,\big[k_s\,(11025-630a_{20}-2100a_{40}+420a_{20}a_{40}-315a_{20}^2)$
	$+k_t\,(2205+630a_{20}-840a_{40}-120a_{20}a_{40}+45a_{20}^2+80a_{40}^2)\big]$
	$+k_nk_s[k_s\,(7350+630a_{20}+2100a_{40}-420a_{20}a_{40}-1890a_{20}^2+294a_{20}^3)$
	$+k_t\,(10290-630a_{20}-1120a_{40}+520a_{20}a_{40}-594a_{20}^2-160a_{40}^2+56a_{20}^2a_{40}-42a_{20}^3)\big]$
	$+k_s^2k_t\,(5880+1960a_{40}-400a_{20}a_{40}-1656a_{20}^2+80a_{40}^2-56a_{20}^2a_{40}+336a_{20}^3)$
E	$2k_n\,(k_n-k_s)\,(2a_{20}+5)\,(5-a_{20})\,(21+3a_{20}-4a_{40})$
F	$-k_n\,(a_{20}-5)^2\,\big[k_s^2k_t\,(3528+1008a_{20}+1596a_{40}+48a_{20}a_{40}-900a_{20}^2-32a_{40}^2)$
	$+k_nk_s\,\big[-k_s\,(6615+2457a_{20}+840a_{40}-168a_{20}a_{40}-756a_{20}^2)$
	$+k_t\,(8379+1449a_{20}-1932a_{40}-96a_{20}a_{40}+36a_{20}^2+64a_{40}^2)\}$
	$-k_n^2\{k_s\,(4410-252a_{20}-840a_{40}+168a_{20}a_{40}-126a_{20}^2)$
	$+k_t\,(882+252a_{20}-336a_{40}-48a_{20}a_{40}+18a_{20}^2+32a_{40}^2)\big]\big]$
G	$252k_nk_sk_t\,(a_{20}-5)^2\,(2a_{20}+5)^2$
H	$k_n\,\big[k_s\,(2625-315a_{20}^2+42a_{20}^3)+k_t\,(3675+1710a_{20}+800a_{40}-160a_{20}a_{40}-477a_{20}^2+8a_{20}^2a_{40}-132a_{20}^3)\big]$
	$+k_tk_s\,(4200+1440a_{20}-800a_{40}-160a_{20}a_{40}+162a_{20}^2-8a_{20}^2a_{40}+6a_{40}^3)$

$$C=\frac{l^2N_p}{90}\begin{bmatrix}\frac{A}{B} & \frac{E}{B} & \frac{E}{B} & 0 & 0 & 0\\ \frac{E}{B} & \frac{C}{D} & \frac{F}{D} & 0 & 0 & 0\\ \frac{E}{B} & \frac{F}{D} & \frac{C}{D} & 0 & 0 & 0\\ 0 & 0 & 0 & \frac{C-F}{2D} & 0 & 0\\ 0 & 0 & 0 & 0 & \frac{G}{H} & 0\\ 0 & 0 & 0 & 0 & 0 & \frac{G}{H}\end{bmatrix}, \tag{27}$$

where the parameters $A\sim H$ are given in Table 1. Note that the parameters $A\sim H$ are introduced here merely to simplify the representation of the stiffness matrix. It is known that in transversely isotropic materials, the Poisson's ratios will be different based on the directions in which they are acting. In Fig. 2, the variations of the two Poisson's ratios (ν_{12} and ν_{23}) are shown with respect to the microscopic parameters, where the ratios of the tangential and normal inter-granular stiffness coefficients are defined as $\beta_s=k_s/k_n$ and $\beta_t=k_t/k_n$. Figure 2 also shows for comparison the Poisson's ratios predicted using an alternative kinematic approach, in which the derivation of the macroscopic stiffness tensor is driven by specifying the inter-granular displacement vector as a projection of macroscale strain tensor and utilizing the Helmholtz energy. A brief discussion of the kinematic approach is presented in Appendix.

The closed-form solutions for Young's modulus, E, and Poisson's ratio, ν, using least squares and kinematic approach have been presented previously by Chang and coworkers as well as others [15,54] and are shown here for reference:

$$E=\frac{5l^2\rho^c}{3}\frac{k_nk_s}{2k_n+3k_s}\quad\text{and}\quad\nu=\frac{k_n-k_s}{2k_n+3k_s}\ \text{(Least squares)}, \tag{28a}$$

$$E=\frac{l^2\rho^c}{3}\frac{k_n(2k_n+3k_s)}{4k_n+k_s}\quad\text{and}\quad\nu=\frac{k_n-k_s}{4k_n+k_s}\ \text{(Kinematic)}. \tag{28b}$$

For the positive values of grain–pair stiffness coefficients, the Poisson ratio is predicted in the range of $-1/3$ to 1/2 for least squares approach and -1.0 to 1/4 for the kinematic approach. From a practical viewpoint, these ranges of Poisson's ratio are valid for many engineering materials. It is also noteworthy that from the viewpoint of positive semi-definiteness of macroscale deformation energy, negative grain–pair stiffness could be admissible. In this case, the whole thermodynamically admissible range of Poisson's ratio (from -1.0 to 0.5) can be modeled with both approaches. At the inter-granular scales, the negative stiffness represents certain mechanisms that are manifested due to the immediate and extended neighborhood. For the least squares approach,

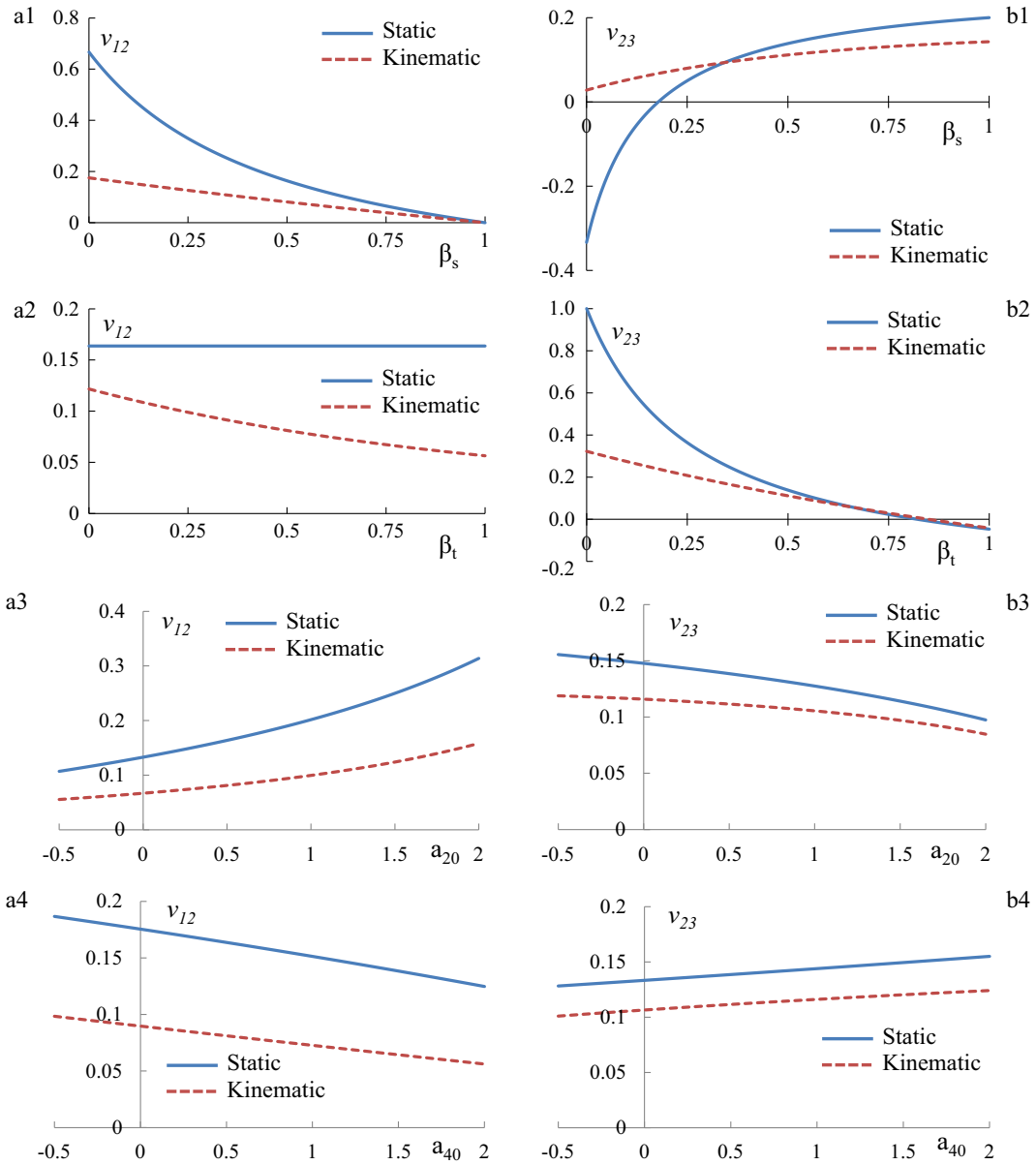

Fig. 2 Variation of the two Poisson ratios of transversely isotropic materials with changing (sections **a1** and **b1**) β_s while $\beta_t = a_{20} = a_{40} = 0.5$; (sections **a2** and **b2**) β_t while $\beta_s = a_{20} = a_{40} = 0.5$; (sections **a3** and **b3**) a_{20} while $\beta_s = \beta_t = a_{40} = 0.5$; (sections **a4** and **b4**) a_{40} while $\beta_s = \beta_t = a_{40} = 0.5$

the normal stiffness must take negative values (up to $-2k_s/3$ for $\nu = -1$). The negative normal stiffness for these highly auxetic materials connotes severe dilation attributable to grain–pair as the grain neighborhood experiences shear. For the kinematic approach, the shear stiffness must take negative values (up to $-2k_n/3$ for $\nu = 0.5$). In this case, the negative shear stiffness for these materials approaching incompressibility implies shear softening attributable to grain–pair as the grain neighborhood experiences compression or extension. We have noted earlier that the inter-granular stiffness coefficients model the effects of immediate neighbors as well as the extended granular microstructure. Such a view is in contrast to the past derivations of these expressions, including expressions for anisotropic materials, in which the inter-granular stiffness coefficients were restrictively taken to represent the stiffness of two isolated grains interacting with each other. Furthermore, the grain–pair behavior can potentially be treated using a volumetric–deviatoric split of normal displacement as in the kinematic constrained microplane model [25]. Such split provides an alternative way to model the thermodynamically admissible range of Poisson's ratio. However, it leads to two different normal stiffness coefficients

(volumetric and deviatoric) in the case of the kinematic approach. Similar volumetric–deviatoric split of shear displacement will likely result in two different shear stiffness in the case of the least squares approach.

6 Elastic wave velocity and effects of model parameters

The velocity of elastic waves propagating within granular and porous media and the effects of material properties thereon has been studied extensively using experimental approaches [61–63] and numerical techniques [64–66]. In this paper, the elastic wave propagation velocity is discussed with the view to show change of material macroscopic behavior resulting from changing microscopic parameters. The velocity surfaces that represent the velocity of waves propagating in different directions through the material have been calculated by varying the microscale parameters. These surfaces are composed of three sheets, one quasi-longitudinal (P) and two quasi-shear waves ($S1$ and $S2$) [67]. The wave velocities in the material are obtained from the Christoffel equation

$$\det\left(\Gamma_{ik} - G\delta_{ik}\right) = 0, \tag{29}$$

where Γ_{ik} is the Christoffel matrix which is derived by contracting the stiffness tensor with the unit normal vector twice given as $C_{ijkl}n_j n_l$. From Eq. (29), it is clear that G is the eigenvalue of the Christoffel matrix and represents phase velocity. By solving the above equation, three eigenvalues of the Christoffel matrix and their corresponding eigenvectors are derived. The biggest eigenvalue belongs to the quasi-longitudinal wave and the two others belong to the shear waves, one being pure shear and the other quasi-shear wave. For each case, the value of wave velocity can be derived as $\Gamma_{ij}g_i g_j$ where $\boldsymbol{g}$ is the corresponding eigenvector [68].

For illustration in this paper, we have calculated the velocity surfaces for transversely isotropic materials for a range of microscale parameters. It is recalled that for transversely isotropic materials, five microscale parameters are used, namely k_n, k_s, k_t, a_{20}, and a_{40}. In Figs. 3, 4, 5 and 6, sections of velocity surfaces with coordinate planes showing the change of elastic wave velocities resulting from varying the values of $\beta_s = k_s/k_n$, $\beta_t = k_t/k_n$, a_{20}, and a_{40}, respectively, are presented. For comparison, the wave velocities have been normalized by k_n. In all these figures, sections a, b, and c represent sections of the velocity surfaces (P, $S1$, and $S2$ waves, respectively) with 12 plane, while sections d, e, and f represent sections of the same surfaces with the 23 plane. It is noted that since the axis 1 is the axis of rotational symmetry, material behavior in all directions inside the plane whose normal vector is axis 1 is identical. Thus, sections of velocity surface only with 12 plane and 23 plane are provided and section of the surface with 31 plane will be exactly same as that with 12 plane. We also note that, because of this rotational symmetry, the velocity surface section with 23 plane will be always a circle regardless of the values of fabric parameters (a_{20} and a_{40}) and ratios of inter-granular stiffness coefficients.

Sections a–f represent results calculated using the kinematic approach, while sections a'–f' show the same results from the least squares approach. It is evident that using same the set of microscale stiffness, the wave velocity computed based on the least squares approach is smaller than that of the kinematic approach. However, the trend of change of velocities resulting from change of microscopic properties is generally similar between the two methods. The exception is seen for the quasi-shear wave, in which discrepancies in the shape of the wave velocity profile derived from the two different methods can be observed. These differences in the results of the two approaches are due to the fact that the two methods use different approaches to link microscale and macroscale kinematic measures, force/stress measures, and material properties. Thus, the efficacy of the two approaches to represent different types of granular solids could be judged by a systematic variation of their average microscale parameters.

From Figs. 3 and 4, we can observe that the tangential stiffness k_s appears to affect the longitudinal velocity more in the 1-direction, while the stiffness k_t primarily influences the behavior in the 23 plane as seen from comparison of Figs. 3a (3a') with 4a (4a'). It is also interesting to see that the tangential stiffness k_t significantly affects the shape of the quasi-shear wave velocity surface as seen in Figs. 3c (3c') and 4c (4c'). The directional density parameters a_{20} and a_{40} also have a significant influence upon the shape of the velocity surfaces in the 12 plane. Thus, by changing the microscale parameters (stiffness and directional density parameters) a wide range of transverse anisotropic behavior can be modeled. Similar anisotropy descriptions can be obtained for materials with other types of inherent anisotropies.

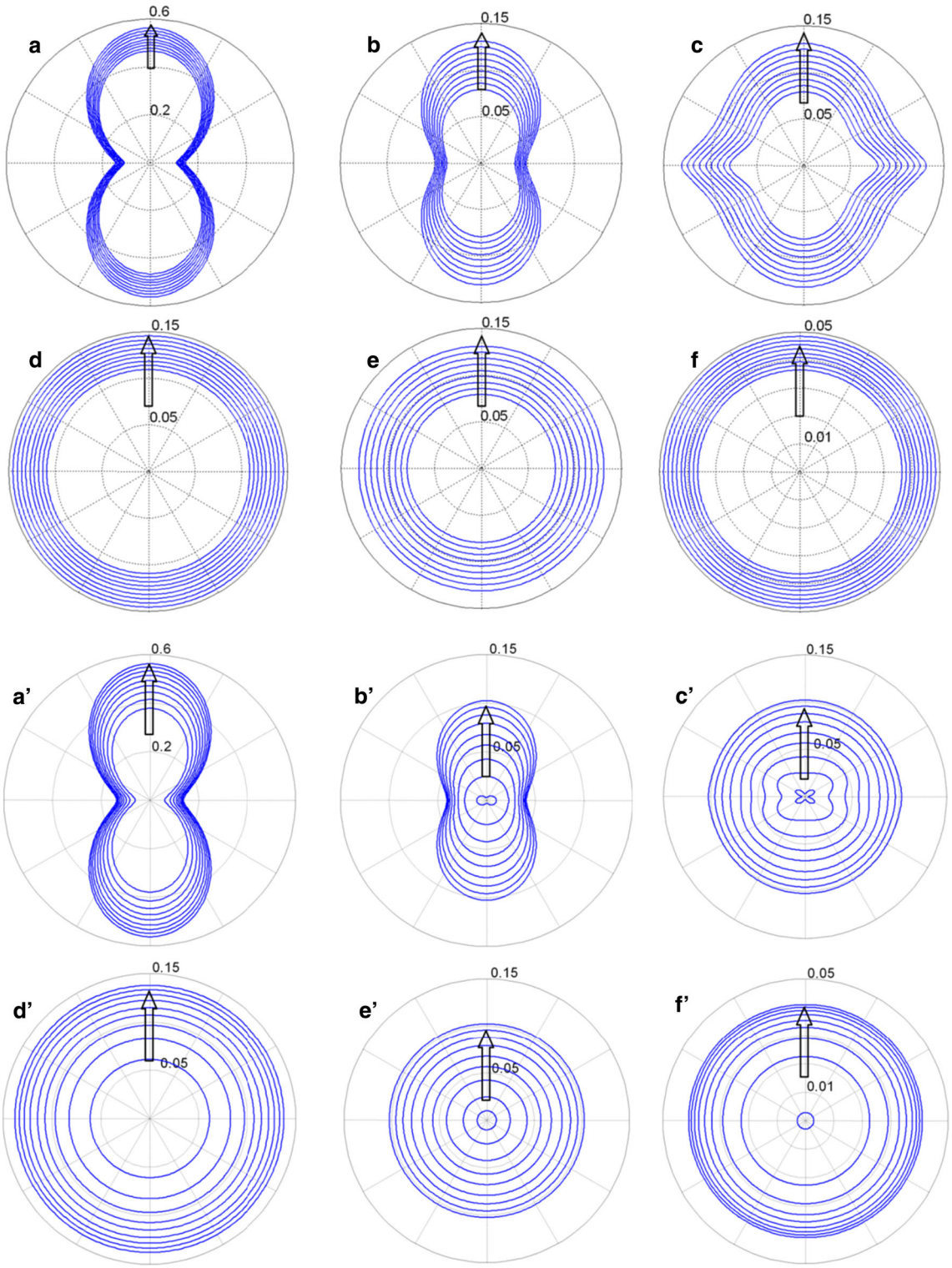

Fig. 3 Sections of the quasi-longitudinal, pure shear and quasi-shear components of wave velocity surface with 12 plane (graphs **a**–**c**, respectively) and with 23 plane (graphs **d**–**f**, respectively) while changing ratio of $\beta_s = 0.1 \sim 0.9$ with $a_{20} = a_{40} = 2.0$, $\beta_t = 0.5$. *Arrows* represent the direction of variation of the surface while increasing β_s. For visualization purposes, the values of wave velocities are reduced by 0.025. Calculations are done with kinematic approach (**a**–**f**) and static approach (**a'**–**f'**)

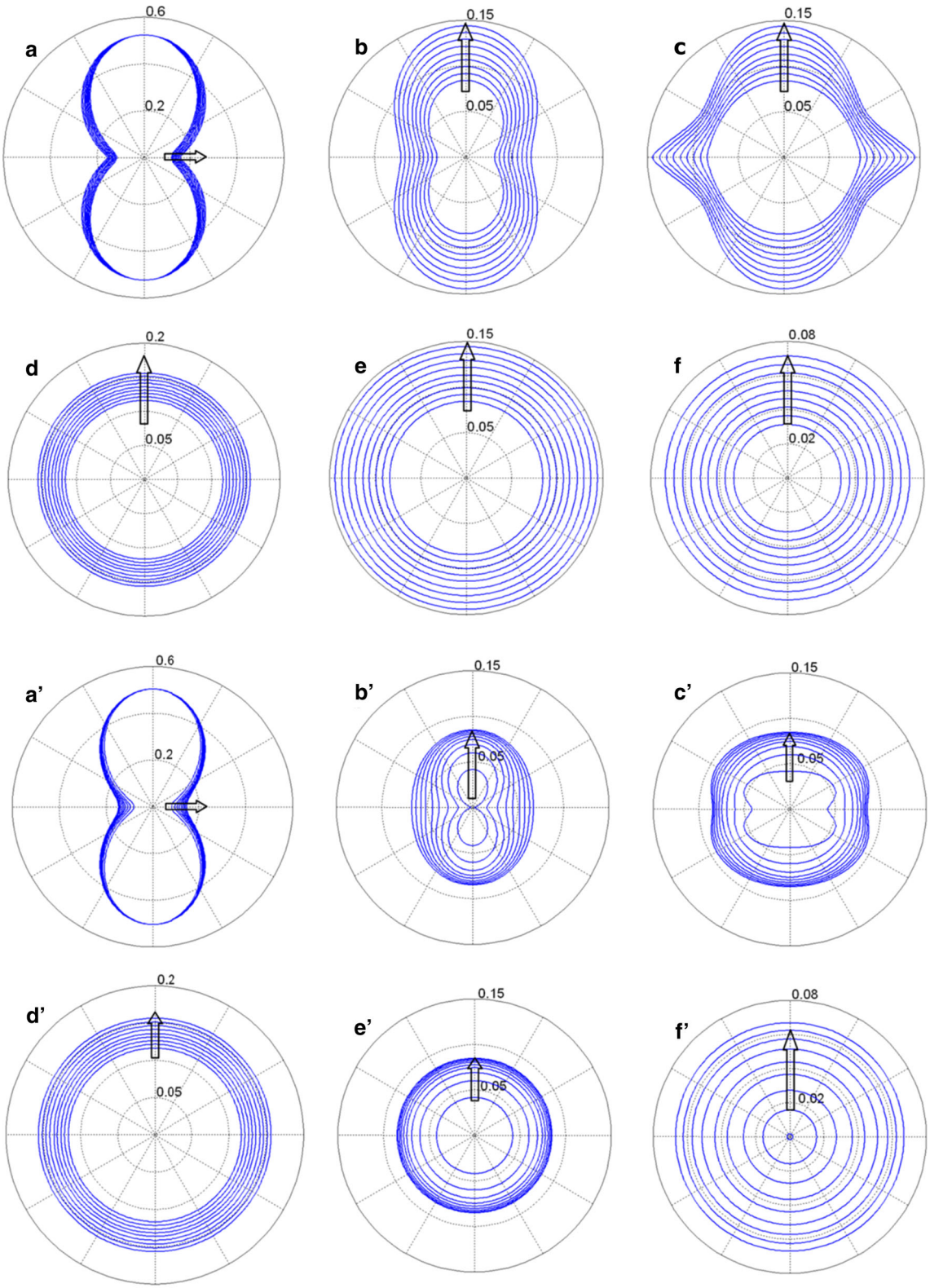

Fig. 4 Sections of the quasi-longitudinal, pure shear and quasi-shear components of wave velocity surface with 12 plane (graphs **a**–**c**, respectively) and with 23 plane (graphs **d**–**f**, respectively) while changing ratio of $\beta_t = 0.1 \sim 0.9$ with $a_{20} = a_{40} = 2.0$, $\beta_s = 0.5$. *Arrows* represent the direction of variation of the surface while increasing β_t. For visualization purposes, the values of wave velocities are reduced by 0.025. Calculations are done with kinematic approach (**a**–**f**) and static approach (**a'**–**f'**)

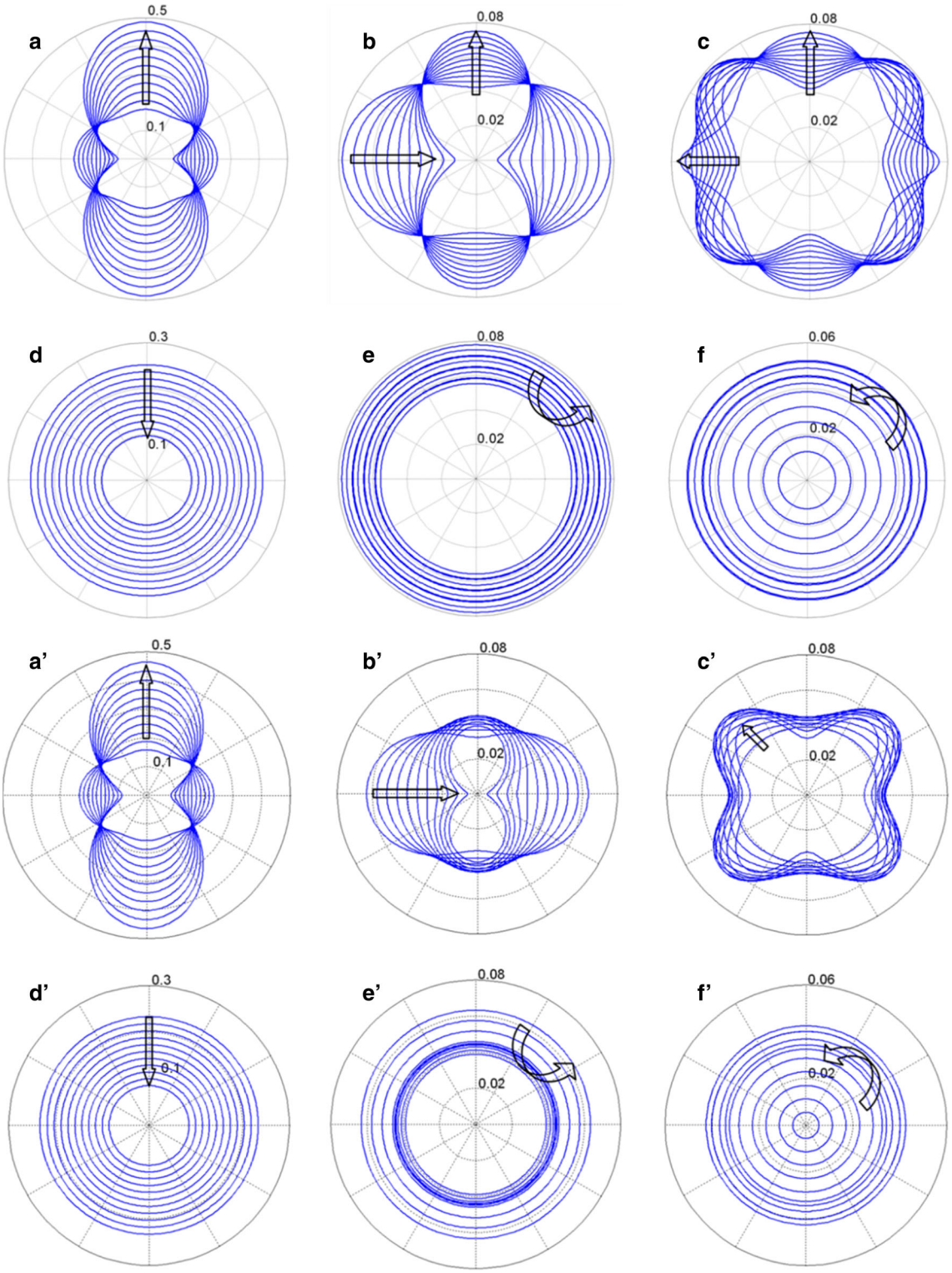

Fig. 5 Sections of the quasi-longitudinal, pure shear and quasi-shear components of wave velocity surface with 12 plane (graphs **a**–**c**, respectively) and with 23 plane (graphs **d**–**f**, respectively) while changing ratio of $a_{20} = -0.5 \sim 2.0$ with $a_{40} = 2.0$, $\beta_s = \beta_t = 0.5$. *Arrows* represent the direction of variation of the surface while increasing a_{20}. For visualization purposes, the values of wave velocities are reduced by 0.025. Calculations are done with kinematic approach (**a**–**f**) and static approach (**a'**–**f'**)

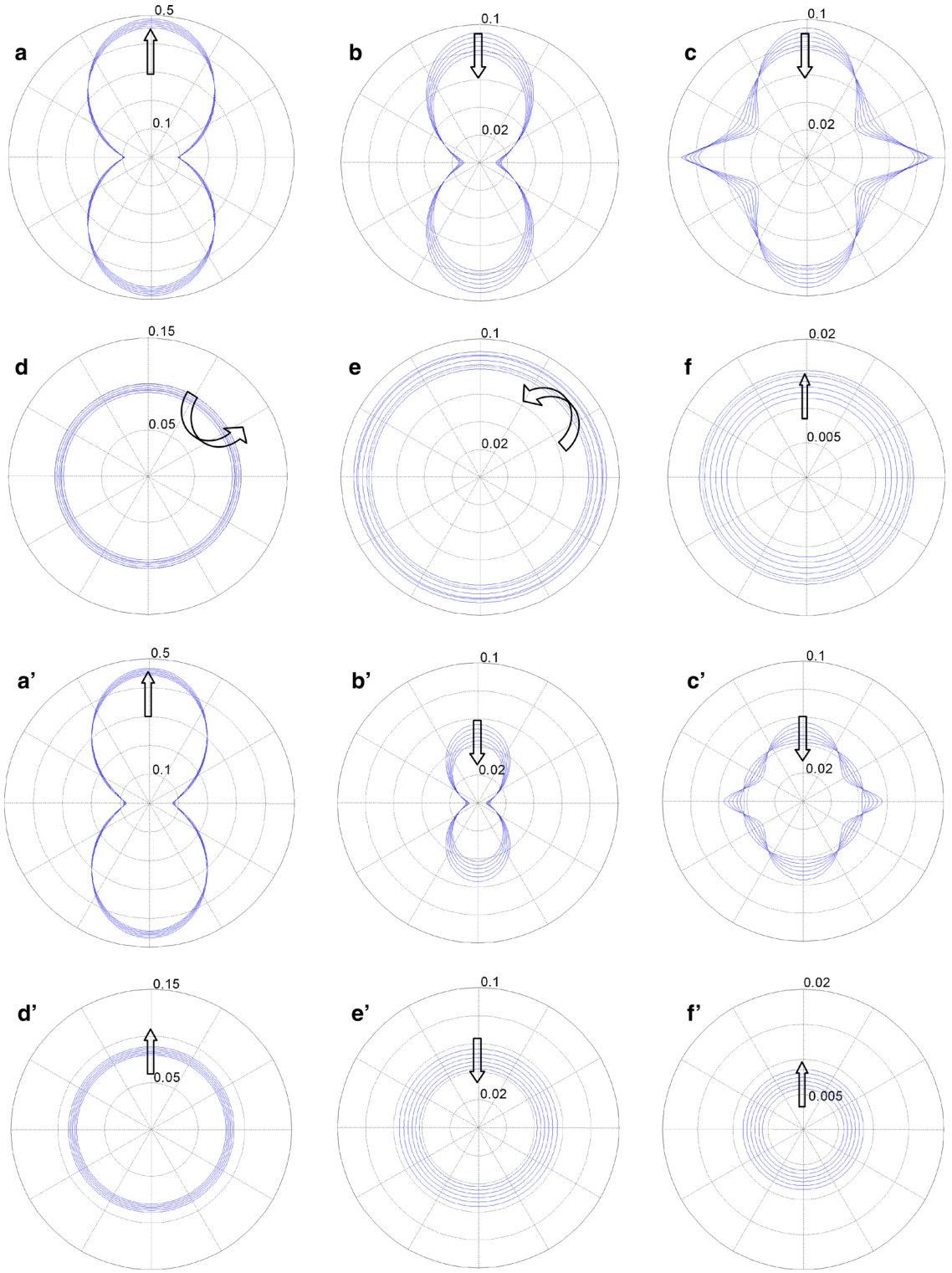

Fig. 6 Sections of the quasi-longitudinal, pure shear and quasi-shear components of wave velocity surface with 12 plane (graphs **a**–**c**, respectively) and with 23 plane (graphs **d**–**f**, respectively) while changing ratio of $a_{40} = -0.5 \sim 2.0$ with $a_{20} = 2.0$, $\beta_s = \beta_t = 0.5$. *Arrows* represent the direction of variation of the surface while increasing a_{40}. For visualization purposes, the values of wave velocities are reduced by 0.025. Calculations are done with kinematic approach (**a**–**f**) and static approach (**a'**–**f'**)

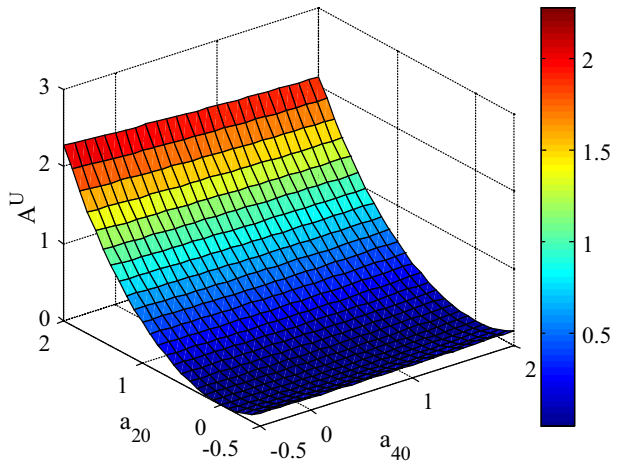

Fig. 7 3D representation of variation of the universal anisotropy index with changing the values of a_{20} and a_{40} while keeping $\beta_s = \beta_t = 0.5$

7 Anisotropy index and effects of model parameters

Materials' elastic anisotropy plays a key role in many mechanical properties. In addition to the elastic behavior, which is obviously affected by anisotropy, other mechanical–physical properties that are affected by elastic anisotropy include, but are not limited to, phase transformations, dislocation dynamics, anisotropic plastic deformation, mechanical yield points, crack behavior, elastic instability, and internal friction [69]. To quantify the measure of anisotropy, a number of scalar measures have been proposed over the years [69–71], but they all have their limitations. Recently, a more general quantitative measure of the degree of anisotropy termed as the universal anisotropy index has been introduced [42], defined as

$$A^{\mathrm{U}} = 5\frac{G^{\mathrm{V}}}{G^{\mathrm{R}}} + \frac{K^{\mathrm{V}}}{K^{\mathrm{R}}} - 6 \geq 0. \tag{30}$$

In Eq. (30), the superscripts V and R represent the Voigt and Reuss estimates of the shear, G, and, bulk, K, moduli respectively. The anisotropy index takes the value of 0 for isotropic materials and positive values for anisotropic materials. In order to calculate this index for anisotropic materials, first the compliance and stiffness matrices for the material are derived. Then, by rotating the material in all generic directions in space and averaging the compliance and stiffness matrices for all directions their corresponding isotropic matrices are calculated. The Voigt estimate of the shear and bulk moduli (G^{V} and K^{V}) of the material is found using the isotropic stiffness tensor, while the Reuss estimate (G^{R} and K^{R}) is found from the compliance matrix. Figure 7 shows the variation of the anisotropy index for different transversely isotropic materials with changing the values of a_{20} and a_{40} while keeping $\beta_s = \beta_t = 0.5$. It is seen that the effects of a_{20} are much larger than those of a_{40}. This is reasonable considering the fact that a_{20} is the coefficient of the first term in the expansion and the higher-order terms have diminishing effects on the anisotropy of the material. The range of values of A^{U} calculated using the results of this model span those of measure hexagonal crystals reported in [42]. It is important to note that this quantitative measure of anisotropy is inherently independent of the material elastic symmetries. Using this measure, it is possible to have a transversely isotropic material with an anisotropy index higher than that of an orthotropic material (as seen in [42] Fig. 2). So the anisotropy index just provides a quantitative measure to evaluate the severity of anisotropic behavior and not the type or degree of anisotropy, which is determined by the presence (or lack) of elastic symmetries.

8 Conclusion

A method for modeling materials with different levels of anisotropy using a Gibbs potential-based granular micromechanics approach has been developed. From the viewpoint of the granular micromechanics approach, the overall classical Gibbs potential of a material point is defined as the volume average of the grain–pair deformation energy, which is taken as a function of the inter-granular forces. In the first-order theory developed

here, (1) the inter-granular forces are related to the Cauchy stress tensor using a modified static constraint that incorporates directional distribution of the grain–pair interactions, and (2) the relationship between inter-granular displacement and the macroscale strain tensor is obtained by considering the conjugate relationship of strain and Cauchy stress. The constitutive relation is then established by using inter-granular stiffness coefficients defined on the basis of the conjugate relationship of inter-granular displacement and forces. The clear implication of the inter-granular stiffness coefficients introduced in this manner is that they are different from that of the isolated grain–pair and model the behavior of a grain–pair embedded in a granular material and represent the effect of immediate neighbors as well as the extended microstructure. They function as parameters that need to be determined as back-calculations from macroscale measurements and not through direct measurements of two isolated grains as in contact mechanics. Further, to establish an integral form for the compliance tensor, two distinct directional density distribution functions are defined; one related to the average directional distribution of number, length, and stiffness/compliance of grain–pair interactions and the other related to average directional distribution of number and length of grain–pair interactions.

Subsequently, for ensuring that the model is capable of reproducing different levels of anisotropy, the distribution density function is parameterized using spherical harmonics expansion with carefully selected terms. It is shown that using the density distribution function with 18 parameters is sufficient for modeling a completely anisotropic material. These 18 directional density parameters along with the three inter-granular stiffness coefficients make a total of 21 independent microscale constants and will result in 21 mutually independent, nonzero components of a 6×6 stiffness matrix.

Different levels of anisotropy in materials arise from planes of elastic symmetry and/or axes of rotational symmetry. In the present paper, the density distribution function is systematically modified for modeling materials with only 1 plane of elastic symmetry, orthotropic materials, and transversely isotropic materials. In all these cases, the derived stiffness matrices are consistent with the symmetry requirements of that particular material. For each anisotropy level, the number of micromechanical parameters is equal to the number of independent constants in the stiffness tensor of that particular anisotropy level. As a measure to demonstrate the effects of change of micromechanical properties included in the model to the macroscopic behavior of the material, the elastic wave propagation velocity through a transversely isotropic material is discussed. The variation of the wave velocity with changing microscopic properties is shown. The results are also compared with those obtained from the method using the kinematic assumption. It is found that the velocity of surface quasi-shear waves can show different trends for the two methods, suggesting that wave propagation can be applied to evaluate the efficacy of the two approaches to represent different types of granular solids.

Acknowledgments This research was supported in part by the United States National Science Foundation grant CMMI-1068528.

Appendix: Least squares approximation

We consider the deviation of the grain–pair relative displacement vector, δ_i, from the projection of the macroscopic strain tensor on the vector joining the grain–pair centroid given as $\varepsilon_{ij} l_j$, and define an error parameter, R_i, as follows:

$$R_i = \sum_{\alpha=1}^{N} R_i^{\alpha} = \sum_{\alpha=1}^{N} \varepsilon_{ij} l_j^{\alpha} - \delta_i^{\alpha}, \tag{31}$$

where the summation is over all the contacts in an RVE. The objective is to minimize the square of the error R_i, which gives

$$\frac{\partial (R_i R_i)}{\partial \varepsilon_{mn}} = \sum_{\alpha=1}^{N} 2 R_i^{\alpha} \frac{\partial}{\partial \varepsilon_{mn}} \left(\varepsilon_{ij} l_j^{\alpha} - \delta_i^{\alpha} \right) = \sum_{\alpha=1}^{N} 2 R_m^{\alpha} l_n^{\alpha} = 0. \tag{32}$$

As a result, the following relationship is obtained between the macroscopic strain tensor and the grain–pair relative displacement vectors:

$$\varepsilon_{mp} = \left(\sum_{\alpha=1}^{N} l_p^{\alpha} l_n^{\alpha} \right)^{-1} \sum_{\alpha=1}^{N} \delta_m^{\alpha} l_n^{\alpha}, \tag{33}$$

which turns out to be identical to Eq. (6). Using Eq. (33) along with the principle of virtual work by equating the virtual work expressed in terms of the macroscopic strain and stress and the grain–pair relative displacement

and force, and assuming linear independence or term-by-term equation of virtual work, the grain pair force can be found as given in Eq. (4) (see for more details [28,37,54]).

Appendix: Kinematic approach

An alternative approach in the granular micromechanics is the method with kinematic constraint [72], in which the inter-granular displacement vector is derived directly by projecting the global strain tensor on the direction of the line joining the centroids of the two neighbor grains. Conjugate to these displacement measures, inter-granular force measures are defined and the relationship between these force and displacement measures are defined using inter-granular stiffness coefficients. Further, the macroscale Helmholtz free energy is obtained as the volume average of grain–pair interaction energies. The macroscopic Cauchy stress is thus defined as the work conjugate of the strain tensor and derived as the derivative of the macroscopic Helmholtz free energy with respect to strain. As a result, material macroscopic stiffness tensor is obtained as follows:

$$C_{ijkl} = \rho^c \int_{\Omega} K_{ik} l_j l_l \xi\,(\theta, \phi) \mathrm{d}\Omega = l^2 \rho^c \int_{\theta=0}^{\pi} \int_{\phi=0}^{2\pi} \left(K_{ik} n_j n_l \xi\,(\theta, \phi)\right) \sin\theta \mathrm{d}\phi \mathrm{d}\theta, \tag{34}$$

where K_{ik} is the inter-granular stiffness matrix and $\xi(\theta, \phi)$ is the directional density distribution function. For modeling materials with different levels of anisotropy using this method, the same procedure used in least squares approach can be applied. In the most general case and for modeling completely anisotropic materials, the method uses three independent inter-granular stiffness coefficients, one for normal direction and two for two tangential directions. Further, the directional density distribution function used in the kinematic approach is defined in the same manner as that used for least squares approach.

References

1. Bayuk, I.O., Ammerman, M., Chesnokov, E.M.: Elastic moduli of anisotropic clay. Geophysics **72**(5), D107–D117 (2007)
2. Graham, J., Houlsby, G.: Anisotropic elasticity of a natural clay. Géotechnique **33**(2), 165–180 (1983)
3. Li, X.S., Dafalias, Y.F.: Constitutive modeling of inherently anisotropic sand behavior. J. Geotech. Geoenviron. Eng. **128**(10), 868–880 (2002)
4. Ochiai, H., Lade, P.V.: Three-dimensional behavior of sand with anisotropic fabric. J. Geotech. Eng. **109**(10), 1313–1328 (1983)
5. Sayers, C., Kachanov, M.: Microcrack-induced elastic wave anisotropy of brittle rocks. J. Geophys. Research (All Ser.) **100**, 4149–4149 (1995)
6. Thomsen, L.: Elastic anisotropy due to aligned cracks in porous rock. Geophys. Prospect. **43**(6), 805–829 (1995)
7. Arthur, J., Chua, K., Dunstan, T.: Induced anisotropy in a sand. Geotechnique **27**(1), 13–30 (1977)
8. Dewhurst, D.N., Siggins, A.F.: Impact of fabric, microcracks and stress field on shale anisotropy. Geophys. J. Int. **165**(1), 135–148 (2006)
9. Horii, H., Nemat-Nasser, S.: Overall moduli of solids with microcracks: load-induced anisotropy. J. Mech. Phys. Solids **31**(2), 155–171 (1983)
10. Jiang, G.-L., Tatsuoka, F., Flora, A., Koseki, J.: Inherent and stress-state-induced anisotropy in very small strain stiffness of a sandy gravel. Geotechnique **47**(3), 509–521 (1997)
11. Johnson, D., Schwartz, L., Elata, D., Berryman, J., Hornby, B., Norris, A.: Linear and nonlinear elasticity of granular media: stress-induced anisotropy of a random sphere pack. J. Appl. Mech. **65**(2), 380–388 (1998)
12. Wong, R., Arthur, J.: Induced and inherent anisotropy in sand. Geotechnique **35**(4), 471–481 (1985)
13. Placidi, L., Greve, R., Seddik, H., Faria, S.H.: Continuum-mechanical, anisotropic flow model for polar ice masses, based on an anisotropic flow enhancement factor. Contin. Mech. Thermodyn. **22**(3), 221–237 (2010)
14. Placidi, L., Hutter, K.: An anisotropic flow law for incompressible polycrystalline materials. Zeitschrift für Angewandte Mathematik und Physik (ZAMP) **57**(1), 160–181 (2005)
15. Chang, C.S., Misra, A.: Packing structure and mechanical-properties of granulates. J. Eng. Mech. ASCE **116**(5), 1077–1093 (1990)
16. Navier, C.L.: Sur les lois de l'equilibre et du mouvement des corps solides elastiques. Memoire de l'Academie Royale de Sciences **7**, 375–393 (1827)
17. Cauchy, A.-L.: Sur l'equilibre et le mouvement d'un systeme de points materiels sollicites par des forces d'attraction ou de repulsion mutuelle. Excercises de Mathematiques **3**, 188–212 (1826–1830)
18. Misra, A., Poorsolhjouy, P.: Granular micromechanics based micromorphic model predicts frequency band gaps. Contin. Mech. Thermodyn., 1–20 (2015). doi:10.1007/s00161-015-0420-y
19. Misra, A., Ching, W.Y.: Theoretical nonlinear response of complex single crystal under multi-axial tensile loading. Sci. Rep. **3**, 1488 (2013). doi:10.1038/srep01488

20. Greene, M.S., Li, Y., Chen, W., Liu, W.K.: The archetype-genome exemplar in molecular dynamics and continuum mechanics. Comput. Mech. **53**(4), 687–737 (2013). doi:10.1007/s00466-013-0925-9
21. Solar, M., Meyer, H., Gauthier, C., Fond, C., Benzerara, O., Schirrer, R., Baschnagel, J.: Mechanical behavior of linear amorphous polymers: Comparison between molecular dynamics and finite-element simulations. Phys. Rev. E **85**(2), 1–14 (2012). doi:10.1103/Physreve.85.021808
22. Silling, S.A., Epton, M., Weckner, O., Xu, J., Askari, E.: Peridynamic states and constitutive modeling. J. Elast. **88**(2), 151–184 (2007)
23. Dell'Isola, F., Andreaus, U., Placidi, L.: At the origins and in the vanguard of peri-dynamics, non-local and higher gradient continuum mechanics. An underestimated and still topical contribution of Gabrio Piola. Mech. Math. Solids (2013). doi:10.1177/1081286513509811
24. Tadmor, E.B., Miller, R.E.: Modeling materials: continuum, atomistic and multiscale techniques. Cambridge University Press, Cambridge (2011)
25. Bazant, Z.P., Prat, P.C.: Microplane model for Brittle-plastic material. 1. Theory. J. Eng. Mech. ASCE **114**(10), 1672–1687 (1988)
26. Gao, H.J., Klein, P.: Numerical simulation of crack growth in an isotropic solid with randomized internal cohesive bonds. J. Mech. Phys. Solids **46**(2), 187–218 (1998)
27. Bazant, Z.P., Caner, F.C.: Microplane model M5 with kinematic and static constraints for concrete fracture and anelasticity. I: theory. J. Eng. Mech. ASCE **131**(1), 31–40 (2005). doi:10.1061/(Asce)0733-9399(2005)131:(31)
28. Chang, C., Gao, J.: Kinematic and static hypotheses for constitutive modelling of granulates considering particle rotation. Acta Mech. **115**(1–4), 213–229 (1996)
29. Taylor, G.I.: Plastic strain in metals. J. Inst. Metals **62**, 307–324 (1938)
30. Kruyt, N., Rothenburg, L.: Kinematic and static assumptions for homogenization in micromechanics of granular materials. Mech. Mater. **36**(12), 1157–1173 (2004)
31. Nicot, F., Darve, F., Group, R.: A multi-scale approach to granular materials. Mech. Mater. **37**(9), 980–1006 (2005)
32. Tordesillas, A., Shi, J., Tshaikiwsky, T.: Stress–dilatancy and force chain evolution. Int. J. Numer. Anal. Methods Geomech. **35**(2), 264–292 (2011)
33. Chang, C.S., Misra, A., Acheampong, K.: Elastoplastic deformation for particulates with frictional contacts. J. Eng. Mech. ASCE **118**(8), 1692–1707 (1992). doi:10.1061/(Asce)0733-9399(1992)118:8(1692)
34. Misra, A., Chang, C.S.: Effective elastic moduli of heterogeneous granular solids. Int. J. Solids Struct. **30**(18), 2547–2566 (1993)
35. Nguyen, N.S., Magoariec, H., Cambou, B.: Local stress analysis in granular materials at a mesoscale. Int. J. Numer. Anal. Methods Geomech. **36**(14), 1609–1635 (2012)
36. Nguyen, N.-S., Magoariec, H., Cambou, B., Danescu, A.: Analysis of structure and strain at the meso-scale in 2D granular materials. Int. J. Solids Struct. **46**(17), 3257–3271 (2009)
37. Misra, A., Poorsolhjouy, P.: Micro–macro scale instability in 2D regular granular assemblies. Contin. Mech. Thermodyn. **27**(1-2), 63–82 (2013). doi:10.1007/s00161-013-0330-9
38. Brocca, M., Bažant, Z.P., Daniel, I.M.: Microplane model for stiff foams and finite element analysis of sandwich failure by core indentation. Int. J. Solids Struct. **38**(44), 8111–8132 (2001)
39. Prat, P., Gens, A.: Microplane formulation for quasibrittle materials with anisotropy and damage. In: Bazant, Z.B., Bittnar, Z., Jirasek, M., Mazars, J. (eds.) Fracture and Damage in Quasibrittle Structures: Experiment, modeling and computation, p. 67 (2004)
40. Cusatis, G., Beghini, A., Bažant, Z.P.: Spectral stiffness microplane model for quasibrittle composite laminates—Part I: theory. J. Appl. Mech. **75**(2), 021009 (2008)
41. Gassmann, F.: Elastic waves through a packing of spheres. Geophysics **16**(4), 673–685 (1951)
42. Ranganathan, S.I., Ostoja-Starzewski, M.: Universal elastic anisotropy index. Phys. Rev. Lett. **101**(5), 055504 (2008)
43. Misra, A., Poorsolhjouy, P.: Identification of higher-order elastic constants for grain assemblies based upon granular micromechanics. Math. Mech. Complex Syst. **3**(3), 285–308 (2015)
44. Auffray, N., Dell'Isola, F., Eremeyev, V., Madeo, A., Rosi, G.: Analytical continuum mechanics a la Hamilton–Piola least action principle for second gradient continua and capillary fluids. Math. Mech. Solids **20**(4), 375–417 (2013). doi:10.1177/1081286513497616
45. Giorgio, I., Grygoruk, R., Dell'Isola, F., Steigmann, D.J.: Pattern formation in the three-dimensional deformations of fibered sheets. Mech. Res. Commun. **69**, 164–171 (2015)
46. Mindlin, R.D.: Micro-structure in linear elasticity. Arch. Ration. Mech. Anal. **16**(1), 51–78 (1964)
47. Maugin, G.A.: Some remarks on generalized continuum mechanics. Math. Mech. Solids **20**(3), 280–291 (2015). doi:10.1177/1081286514544859
48. Dell'Isola, F., Seppecher, P.: The relationship between edge contact forces, double forces and interstitial working allowed by the principle of virtual power. Comptes Rendus De L Academie Des Sciences Serie Ii Fascicule B-Mecanique Physique Chimie Astronomie **321**(8), 303–308 (1995)
49. Dell'Isola, F., Seppecher, P.: Edge contact forces and quasi-balanced power. Meccanica **32**(1), 33–52 (1997)
50. Dell'Isola, F., Seppecher, P.: Hypertractions and hyperstresses convey the same mechanical information. Contin. Mech. Thermodyn. **22**, 163–176 (2010) by Prof. Podio Guidugli and Prof. Vianello and some related papers on higher gradient theories. Contin. Mech. Thermodyn. **23**(5), 473–478 (2011). doi:10.1007/s00161-010-0176-3
51. Dell'Isola, F., Seppecher, P., Madeo, A.: How contact interactions may depend on the shape of Cauchy cuts in *N*-th gradient continua: approach "a la D'Alembert". Zeitschrift für Angewandte Mathematik und Physik (ZAMP) (2012). doi:10.1007/s00033-012-0197-9
52. Chang, C.S., Chao, J.S., Chang, Y.: Estimates of elastic moduli for granular material with anisotropic random packing structure. Int. J. Solids Struct. **32**(14), 1989–2008 (1995)
53. Liao, C.L., Chang, T.P., Young, D.H., Chang, C.S.: Stress–strain relationship for granular materials based on the hypothesis of best fit. Int. J. Solids Struct. **34**(31–32), 4087–4100 (1997). doi:10.1016/S0020-7683(97)00015-2

54. Chang, C.S., Liao, C.L.: Estimates of elastic modulus for media of randomly packed granules. Appl. Mech. Rev. **47**(1), 197–206 (1994)
55. Misra, A., Poorsolhjouy, P.: Granular micromechanics model for damage and plasticity of cementitious materials based upon thermomechanics. Math. Mech. Solids (2015). doi:10.1177/1081286515576821
56. Misra, A., Singh, V.: Micromechanical model for viscoelastic materials undergoing damage. Contin. Mech. Thermodyn. **25**(2–4), 343–358 (2013). doi:10.1007/s00161-012-0262-9
57. Misra, A., Singh, V.: Nonlinear granular micromechanics model for multi-axial rate-dependent behavior. Int. J. Solids Struct. **51**(13), 2272–2282 (2014). doi:10.1016/j.ijsolstr.2014.02.034
58. Voigt, W.: Lehrbuch der kristallphysik (mit ausschluss der kristalloptik). Springer, Berlin (2014)
59. Malvern, L.E.: Introduction to the mechanics of a continuous medium. vol. Monograph. Prentice-Hall, New York (1969)
60. Nye, F.: Physical properties of crystals. Clarendon Press, Oxford (1964)
61. Hardin, B.O., Richart Jr., F.: Elastic wave velocities in granular soils. J. Soil Mech. Found. Div. **89** (Proceedings Paper 3407) (1963)
62. Wyllie, M., Gregory, A., Gardner, G.: An experimental investigation of factors affecting elastic wave velocities in porous media. Geophysics **23**(3), 459–493 (1958)
63. Wyllie, M.R.J., Gregory, A.R., Gardner, L.W.: Elastic wave velocities in heterogeneous and porous media. Geophysics **21**(1), 41–70 (1956)
64. Leibig, M.: Model for the propagation of sound in granular materials. Phys. Rev. E **49**(2), 1647 (1994)
65. Melin, S.: Wave propagation in granular assemblies. Phys. Rev. E **49**(3), 2353 (1994)
66. Somfai, E., Roux, J.-N., Snoeijer, J.H., Van Hecke, M., Van Saarloos, W.: Elastic wave propagation in confined granular systems. Phys. Rev. E **72**(2), 021301 (2005)
67. Datta, S., Shah, A.: Elastic waves in composite media and structures. CRC Press, Boca Raton (2009)
68. Vavrycuk, V.: Calculation of the slowness vector from the ray vector in anisotropic media. Proc. R. Soc. A Math. Phys. Eng. Sci. **462**(2067), 883–896 (2006). doi:10.1098/rspa.2005.1605
69. Ledbetter, H., Migliori, A.: A general elastic-anisotropy measure. J. Appl. Phys. **100**(6), 063516 (2006)
70. Chung, D., Buessem, W.: The elastic anisotropy of crystals. J. Appl. Phys. **38**(5), 2010–2012 (1967)
71. Zener, C.: Elasticity and anelasticity of metals. University of Chicago press, Chicago (1948)
72. Misra, A., Yang, Y.: Micromechanical model for cohesive materials based upon pseudo-granular structure. Int. J. Solids Struct. **47**(21), 2970–2981 (2010). doi:10.1016/j.ijsolstr.2010.07.002